



**PHOENICS – YOUR GATEWAY TO CFD SUCCESS**

## Visit to CHAM by Mr Fan Jinglong, CEO of Shanghai-Feiyi



Mr Fan Jinglong of Shanghai Feiyi visited CHAM in April to meet Professor Brian Spalding and others of his team.

Shanghai Feiyi is the exclusive agency for PHOENICS across mainland China and, leaving aside the CHAM UK and CHAM Japan offices, Shanghai Feiyi is the most successful distributor of CHAM software worldwide.

Discussions focussed upon the creation of new special-purpose low-cost VR and SimScene (Simulation Scenario) variants of PHOENICS designed to address the emerging industrial standards and other special requirements identified for particular sectors of the Chinese market.

These include a new specialist fire and smoke modeller to supplement the new **Urban-VWT** (Urban Virtual Wind Tunnel) SimScene recently developed for air ventilation assessment (AVA) studies.

PHOENICS Direct, via which SimScenes are run, is a simplified user interface for CHAM's PHOENICS CFD software package designed for application-specific tasks, without the need for users to gain specialist CFD knowledge or training.

Urban-VWT embodied within PHOENICS Direct simulates wind flow around buildings and other structures. Its menu-based interface leads the user directly to only the capabilities required and produces needed results in a pre-defined form.

Urban-VWT is intended for architects, building engineers, urban planners, local authorities and environment engineers.

It enables users to visualise, investigate, understand, evaluate and refine the air-flow patterns in both micro-and macro-scale.



*Aerial view – selection of area of interest for Urban VWT simulation*

Other SimScenes available for download include:

**F1 VWT**, used by students involved in the F1 in Schools Programme: [www.f1inschools.com](http://www.f1inschools.com);

**HeatEx** for simulation of shell-and-tube heat exchangers: [http://www.cham.co.uk/phoenics/d\\_s/apps/heatex/docs/descr\\_en.htm](http://www.cham.co.uk/phoenics/d_s/apps/heatex/docs/descr_en.htm)

See page 2 for a more detailed description of **Urban-VWT**. For further information about SimScenes in general contact [sales@cham.co.uk](mailto:sales@cham.co.uk), or ring +44 (0)20 8947 7651.

# Urban-VWT SimScene application: Urban Wind Flow

Marta Camps (mcs@cham.co.uk)

## Introduction

Urban-VWT (Urban-Virtual Wind Tunnel) is an application-specific SimScene that uses PHOENICS-Direct as its user interface. It is a tool to assess the effect of wind around buildings and other structures and its impact upon pedestrians and the surrounding cityscape.

In the example shown below, Urban-VWT is used to simulate air flow through a group of buildings in the Zhejiang Province of China.

The focus is on the wind at pedestrian level, especially around the building circled on Fig 1 for North (N) and East-South-East (E-S-E) wind directions.

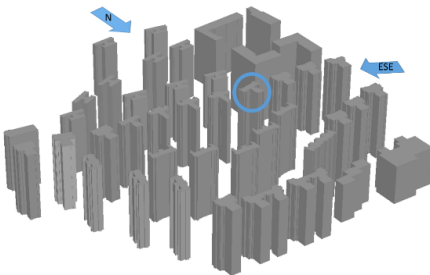


Fig 1 Geometry of the simulation.

## Simulation requirements

The particular region of interest is around the central building and up to 10m above ground. The circle marks the building and the arrows show the two wind directions simulated. In this example, the wind speed is 5m/s at a height of 10m and the roughness height is 0.03m.

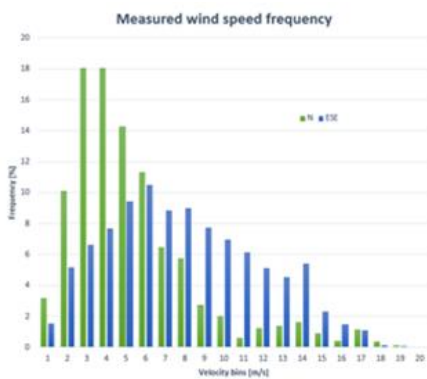


Fig 2 Probability of each wind speed for N & ESE winds

Fig 2 shows a histogram of the measured frequency of each wind direction modelled. Each velocity value shown is the upper limit of its interval.

## Simulation setup

Urban-VWT menus contain all parameters needed to configure a simulation. The setup displayed takes ~ 10 minutes to create.

Urban-VWT's user interface presents 7 parameter groups as buttons on the left hand side. Fig 3 shows the *wind and terrain* group which contains incoming wind characteristics (i.e. 0° wind direction, degrees (0-360°), so N wind) and terrain roughness.

For an E-S-E wind direction the user merely has to change the *wind direction degrees* parameter to 112.5°. The new configuration will be applied and a computational grid for an E-S-E wind will be regenerated automatically and aligned with the wind direction to avoid numerical-diffusion inaccuracies.

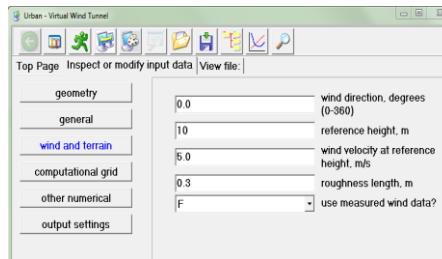


Fig 3 Wind and terrain parameters

Fig 4 displays the *computational grid* group controlling grid resolution and maximum computational cell number. In the present model maximum cell number is 15 million. The smallest cell size is 0.5m in each direction.

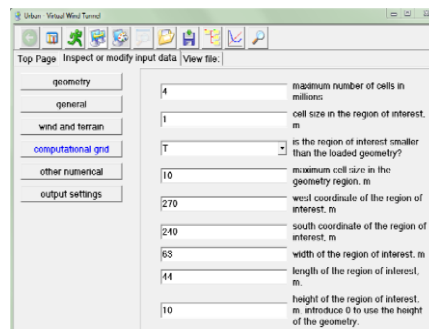
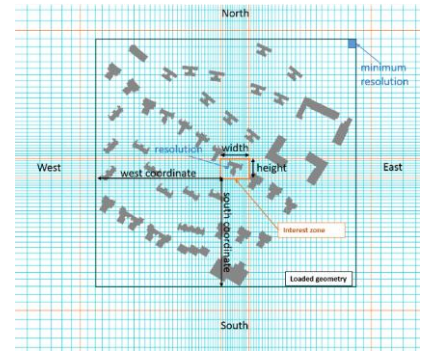


Fig 4 Computational grid parameter group (above) and Graphical representation of its parameters (below).



This resolution is uniformly applied in the interest zone surrounding the building circled in Fig 1 up to 10m above ground level. Cell size expands to 8m for the remainder of the built-up area, with further expansion towards domain boundaries. All values can be changed using the menu and their effect on the grid viewed.

Fig 5 and Fig 6 below display generated grids for N and E-S-E wind directions.

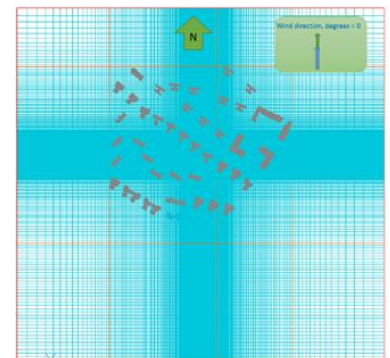


Fig 5 Domain, geometry and mesh generated – N wind



Fig 6 Close up of interest area for E-S-E wind

The remaining groups shown in Fig 3 and 4 above are: *general*, which sets the title of the simulation and the size of its domain; *geometry*, which imports the file with the geometry and configures it; *other numerical* which contains the number of sweeps and processors; *output settings* which controls the automatic post-processing of results.

Clicking 'Run the simulation' will launch the solver and begin the simulation. Once finished, clicking on 'Display results graphically' will generate 2D and 3D plots previously configured in *output settings*.

**Results**

Figures 7, 8, 9 and 10 show results for the E-S-E wind generated by the post-processing feature. In this case, the *output settings* parameter group has been set to generate plots of:

- 1) Fig 7 and Fig 8: Wind Amplification Factor (WAF) @ 2m above ground; where WAF is ratio between wind speed with and without buildings.
- 2) Fig 9: Probability of the wind speed (PRO) to exceed 6m/s @ 2m above ground. Plot generated in conjunction with E-S-E wind data.
- 3) Fig 10: Streamlines started @ 2m above ground.

Images generated are oriented the same way regardless of wind direction. Custom plots can be generated using the standard VR-viewer.

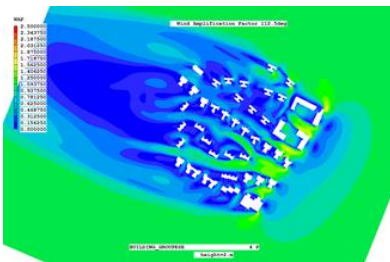


**Fig 7 Wind Amplification Factor contours @ 2m above ground for E-S-E wind**

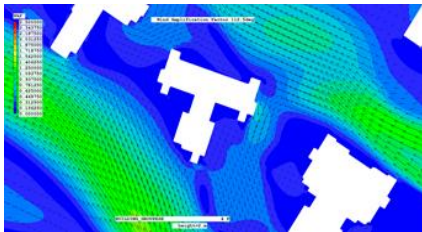


**Fig. 8 Zoom image – Wind Amplification Factor Contours with wind velocity vectors @ 2m above ground for E-S-E wind**

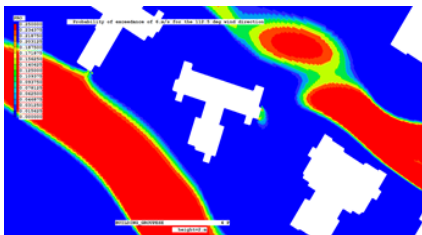


**Fig 9 Contours of probability of the wind speed to exceed 6m/s @ 2m above ground for E-S-E. Red denotes values of 0.25 (ie 25%) or higher**

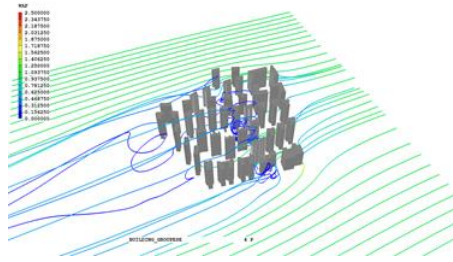


**Fig 10 Streamlines started @ 2m above ground coloured by Wind Amplification Factor for E-S-E wind**

**Summary**

Urban-VWT is designed to model air flow around structures and buildings. The results display meaningful variables used in pedestrian wind comfort studies, allowing the user to extract valuable information without the need for specialist CFD knowledge.

**CFD Modelling of Supercritical Water Heat Transfer in a Vertical Bare Tube Upward Flow**

- [Vladimir Agranat \(vlad@acfa.org\)](mailto:vlad@acfa.org)
- [Michael Malin \(mrm@cham.co.uk\)](mailto:mrm@cham.co.uk)
- [Igor Pioro \(igor.pioro@uoit.ca\)](mailto:igor.pioro@uoit.ca)
- [Rand Abdullah \(Rand.Abdullah@uoit.ca\)](mailto:Rand.Abdullah@uoit.ca)
- [Vladimir Perminov \(valerperminov@gmail.com\)](mailto:valerperminov@gmail.com)

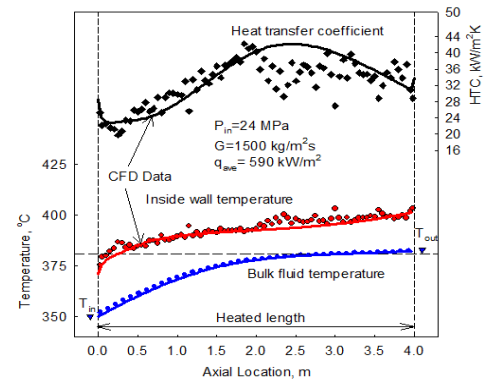
**Abstract**

A customized Computational Fluid Dynamics (CFD) model of supercritical water (SCW) heat transfer in a vertical tube upward flow is developed and partially validated using experimental data obtained under operating conditions typical for SCW cooled reactors (SCWRs): at a pressure of 24 MPa, an inner tube diameter of 10 mm, an inlet temperature of 320 or 350 °C and a heated tube length of 4 m. The three values of mass flux (500, 1000 and 1500 kg/m<sup>2</sup>s) and various values of wall heat flux (from 141 to 729 kW/m<sup>2</sup>) are considered.

SCW physical properties are calculated using REFPROP software from the National Institute of Standards and Technology (NIST). The model was incorporated into the commercial general-purpose CFD software,

PHOENICS, by making extensive use of the INFORM facility. Various turbulence models and numerical grid settings are tested. Use of the double-precision CFD solver is important to obtain complete convergence.

The study demonstrated good agreement between CFD predictions and experimental data on the inside tube wall temperature and heat transfer coefficient using a two-layer low-Reynolds-number k-ε turbulence model. Further model development is required under conditions of significant effects of buoyancy force on heat transfer characteristics (low values of mass flux and high values of wall heat flux). Recommendations are made regarding model applications in analyses of SCWRs.



A typical picture showing comparison of PHOENICS predictions with experimental data is provided above. The full paper will be published in the Proceedings of ICONE 23 (23<sup>rd</sup> International Conference on Nuclear Engineering, May 17-21, 2015, Chiba, Japan). Additional information is available from [info@acfa.org](mailto:info@acfa.org).

**News**

**Safe Solutions Agent for Brazil**

A workshop is being organized, on May 25, at UFSC (Florianópolis) to discuss PHOENICS. It will be attended by teachers and students from Engineering and Architecture. Information will be provided on uses of PHOENICS and there will be opportunities to discuss activities being undertaken by those present. For further information contact [fabio.fundo@safesolutions.com.br](mailto:fabio.fundo@safesolutions.com.br)

## Development of a MATLAB utility for erosion prediction with PHOENICS

Gianandrea Vittorio Messa, Stefano Malavasi  
Politecnico di Milano, Milano, Italy

Impact erosion, ie the loss of material caused by the impingements of solid particles dragged by a fluid, is a serious concern in many engineering applications. It is relevant in the oil & gas industry, because extracted fluids are commonly accompanied by solids, typically sand, having considerable erosive potential. Choke valves used to control the flow on the risers are particularly vulnerable to erosion, and the most significant erosion-related issues are identification of erosion hotspot locations and estimation of loss of material from the valve under aggressive flow conditions.

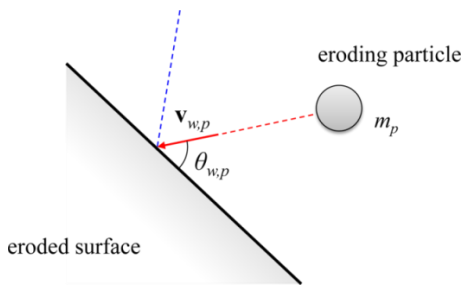


Figure 1 An eroding particle hitting a surface.

Since performing field and lab erosion testing for providing erosion characterization of a control valve is difficult due to economic and technical difficulties, the two above mentioned tasks are usually accomplished with the help of CFD. In particular, use is typically made of single-particle algebraic erosion correlations, which treat the erosion process in terms of the interaction between a single particle and the eroding surface, and express the mass of eroded material removed,  $E_p$ , as a function of the particle mass,  $m_p$ , the modules of the particle impact speed vector,  $|\mathbf{v}_{w,p}|$ , the particle impact angle,  $\vartheta_{w,p}$ , and some properties of the materials involved in the erosion process (Fig. 1). In the application example reported in this brief paper, use is made of the DNV erosion correlation [1], which is one of the most commonly used in the oil&gas industry. The DNV correlation is as follows:

$$E_p = m_p K |\mathbf{v}_{p,w}|^n F(\theta_{w,p}) \quad F(\theta_{w,p}) = \sum_{i=1}^8 A_i \theta_{w,p}^i$$

where  $K$  and  $n$  are constants depending on the material and the  $A_i$  coefficients are given in [1].

The fluid dynamic properties of the particles at the impact stage,  $|\mathbf{v}_{w,p}|$  and  $\vartheta_{w,p}$ , are obtained from two-phase flow simulations based on the Eulerian-Lagrangian approach, in which the fluid is simulated in an Eulerian framework (i.e. cell-based), and, afterwards, the solid phase is represented in a Lagrangian framework by tracking the trajectories of a certain number of parcels (i.e. group of particles sharing the same fluid-dynamic properties). In steady-state flow computations, each parcel has its own mass flow rate,  $\dot{m}_p$ .

Research is being carried out at the Hydraulic Engineering section of the Dept of Civil and Environmental Engineering of Politecnico di Milano regarding erosion in hydraulic equipment such as control valves. In this context, we have recently developed a MATLAB utility for estimating the loss of material from a solid surface starting from the outcomes of an Eulerian Lagrangian two-phase flow simulation performed using the GENTRA add on of PHOENICS. The developed utility requires as input the parcels' characteristics at the impact stage, which can be produced by introducing FORTRAN coding in subroutine GENIUS. The valve surface is triangulated and each impact point is associated to the nearest centroid of the surface elements. Application of an erosion correlation in which the particle mass  $m_p$  is replaced by the parcel mass flow rate  $\dot{m}_p$  yields the mass flux of eroded material removed by the current parcel. The sum over the tracked parcels yields the erosion rate of each surface element, which, once divided by the product of the surface element area and the wall density, produces the local penetration rate (mm/year).

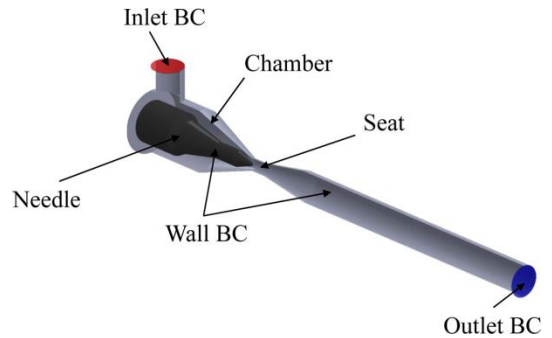


Figure 2 The numerical setup for the valve case.

The procedure has been employed for erosion prediction in abrasive jet tests and in a choke valve, and the results obtained will be presented at the Industrial Valve Summit in Bergamo (Italy) next May and at the ASME Pressure Vessels and Piping Conference PVP2015 in Boston next July.

We will briefly report the outcomes for the valve case. The considered device is sketched in Fig. 2, and relies on the sliding of a needle in a seat to control the flow rate. The valve has a size of 50.8 mm (2 in). The continuous phase is water at 20°C, treated as incompressible, and the solid phase consists of sand particles with density of 2700 kg/m<sup>3</sup> and diameter of 440 μm. At the inlet section, the average velocity of liquid and particles is 7 m/s, and the solid volume fraction is 1%.

Due to the low solid loading, the two-phase flow has been modeled under the hypothesis of “one-way coupling” regime, i.e. by assuming that the liquid affects the motion of the particles but not vice-versa. Therefore, the simulation of the single-phase flow of the liquid phase was followed by a single call to GENTRA to determine the parcels' trajectories. Based on a literature survey, we employed the  $k-\epsilon$  standard turbulence model for evaluating the Reynolds stress tensor of the liquid phase, and, in particle tracking, we included drag and pressure forces and activated the stochastic particle turbulence model available as a GENTRA option.

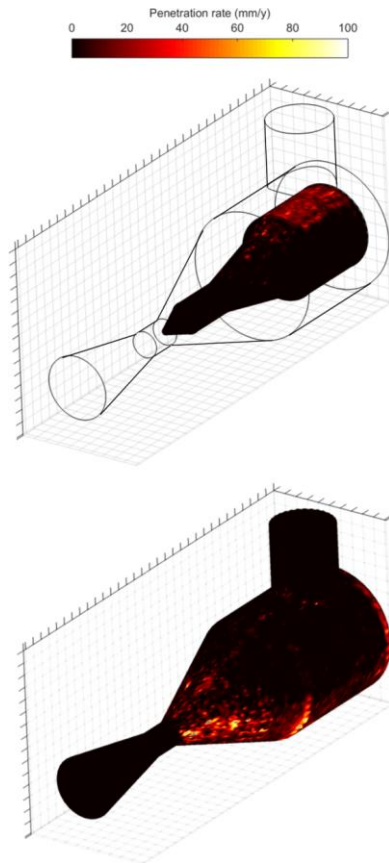


Figure 3 Distribution of the local penetration rate within the valve body estimated by employing the DNV erosion correlation [1].

The developed MATLAB utility was employed to determine the erosion of the valve surface, and specific tests indicated that 100.000 parcels' trajectories were needed to attain statistically representative predictions. Figure 3 shows the distribution of the local penetration rate (i.e. the speed at which the valve surface is removed due to erosion) over the valve body, as obtained from the DNV erosion correlation [1].

The simulation allows clear identification of the locations at which erosion is most likely to occur, which are the part of the needle in front of the inlet pipe and the reducer upstream the cage; this result is compatible with the outcomes of earlier experiments performed on a similar geometry [2]. As part of this research we also intend to perform experimental erosion tests on control devices in our Hydraulic Laboratory [3]. This will allow disposing of experimental data for validating and improving the accuracy of our CFD predictions.

**References**

- [1]. DNV, 2007, Recommended Practice RP O501 Erosive Wear in Piping Systems.
- [2]. Nøkleberg, L., and Søntvedt, T., 1998, Erosion of oil&gas industry choke valves using computational fluid dynamics and experiment, Int. J. Heat Fluid Flow, 19, pp. 636-643.
- [3]. <http://www.dica.polimi.it/laboratori/fantoli/>

## INFORM: Implementation of the Realisable k-ε Turbulence Model

Michael Malin, CHAM

### Introduction

During the last decade the realisable k-ε model [1] has become increasingly popular in the CFD community due to its improved performance over the standard k-ε model when applied to flows involving boundary layers in strong adverse pressure gradients, separation and recirculation zones. The model is also reported to improve significantly the predicted spreading rates of round jets. Several PHOENICS users have expressed an interest in using this model to simulate wind engineering applications involving flow around buildings, where flow separation and recirculation is a major feature.

This two-equation high-Reynolds-number turbulence model differs from the standard k-ε model in two respects. It employs a different formulation of the transport equation for the dissipation rate that is derived from the transport equation for the mean-square vorticity fluctuations. The model also uses a different eddy viscosity formulation based on several realisability constraints for the turbulent Reynolds stresses. In practice this means that the eddy-viscosity coefficient  $C_\mu$  is a function of local flow parameters, rather than a constant, as in the standard k-ε model.

### Turbulence-model equations

The realisable k-ε model is defined by the following equations:

$$\frac{\partial}{\partial t}(\rho k) + \frac{\partial}{\partial x_j}(\rho k u_j) = \frac{\partial}{\partial x_j} \left[ \left( \mu + \frac{\mu_t}{\sigma_k} \right) \frac{\partial k}{\partial x_j} \right] + P_k - \rho \epsilon \tag{1}$$

$$\frac{\partial}{\partial t}(\rho \epsilon) + \frac{\partial}{\partial x_j}(\rho \epsilon u_j) - \frac{\partial}{\partial x_j} \left[ \left( \mu + \frac{\mu_t}{\sigma_\epsilon} \right) \frac{\partial \epsilon}{\partial x_j} \right] = \rho C_1 S \epsilon - \rho C_2 \frac{\epsilon^2}{k + \sqrt{\nu \epsilon}} \tag{2}$$

where  $\sigma_k=1$ ,  $\sigma_\epsilon=1.2$  and  $C_2=1.9$ , and the production rate of turbulent kinetic energy  $P_k$  is given by

$$P_k = \mu_t S^2, \quad S = \sqrt{2 S_{ij} S_{ij}}, \quad S_{ij} = \frac{1}{2} \left( \frac{\partial u_i}{\partial x_j} + \frac{\partial u_j}{\partial x_i} \right) \tag{3}$$

The model coefficient  $C_1$  is computed from:

$$C_1 = \max \left[ 0.43, \frac{\eta}{\eta + 5} \right], \quad \eta = S \frac{k}{\epsilon} \tag{4}$$

and the turbulent dynamic viscosity is calculated from

$$\mu_t = \rho C_\mu \frac{k^2}{\epsilon} \tag{5}$$

Where

$$C_\mu = \frac{1}{A_0 + A_s \frac{k U^*}{\epsilon}}, \quad U^* = \sqrt{S_{ij} S_{ij} + \Omega_{ij} \Omega_{ij}}, \quad \Omega_{ij} = \frac{1}{2} \left( \frac{\partial u_i}{\partial x_j} - \frac{\partial u_j}{\partial x_i} \right) \tag{6}$$

and the model coefficients  $A_0$  and  $A_s$  are given by  $A_0=4.04$  and  $A_s = \sqrt{6} \cos \phi$

where

$$\phi = \frac{1}{3} \cos^{-1} \left( \max(-1, \min(\sqrt{6} W, 1)) \right), \quad W = \frac{S_{ij} S_{jk} S_{ki}}{\tilde{S}^3}, \quad \tilde{S} = \sqrt{S_{ij} S_{ij}} \tag{8}$$

**INFORM Implementation**

The implementation of the model in PHOENICS was made rather easy by using the powerful PIL and INFORM facilities in the Q1 input file. The strategy employed was to activate the built-in standard k-ε turbulence model, and then deactivate built-in source and sink terms for ε, and replace them with the source and sink terms appearing in equation (2) by means of the INFORM (*source of...*) command.

The INFORM (*property ENUT....*) command was then used to compute the eddy viscosity from equation (5) with variable C<sub>μ</sub>. The various model coefficients and tensors appearing in equations (3), (4) and (6) to (8) were computed via the INFORM (*stored of..*) command.

These calculations were facilitated by activating built-in whole-field storage of turbulent frequency EPKE, mean rate of strain GEN1, and various velocity derivatives, e.g. STORE(DUDX,DVDY,... etc. For simplicity and ease of verification, 3d storage was used for the majority of the parameters appearing in the functional relationship for C<sub>μ</sub>, and so there is scope to reduce the storage requirements of the model implementation.

Wall boundary conditions for the momentum, k and ε equations were handled by the default facilities available in PHOENICS for PLATE and BLOCKAGE objects.

To illustrate PIL and INFORM coding, the sequence used to implement the turbulence source terms is given below:

```
REAL(C2E);C2E=1.9
(stored of S is GEN1^0.5 with IMAT<100!ZSLSTR)
(stored of ETA is S/EPKE with IMAT<100!ZSLSTR)
(stored of C1E is max(0.43,ETA/(ETA+5.0)) with
IMAT<100!ZSLSTR)
(stored of ETRM is (ENUL*EP)^0.5 with IMAT<100!ZSLSTR)
(stored of COEP is :C2E:/(KE+ETRM+1.E-10) with
IMAT<100!ZSLSTR)
(Stored of VAEP is C1E*S/COEP with IMAT<100!ZSLSTR)
* Deactivate standard EP source term
COVAL(KESOURCE,EP,ZERO,ZERO)
* Realisable EP source terms
INTEGER(EPLIN);EPLIN=1
IF(EPLIN.EQ.0) THEN
** simple linearisation
(source of EP at KESOURCE is COVAL(COEP*EP,VAEP))
ELSE
** alternative linearisation
(source of EP at KESOURCE is COVAL(FIXFLU,C1E*S*EP))
PATCH(KES2,PHASEM,1,NX,1,NY,1,NZ,1,LSTEP)
(source of EP at KES2 is COVAL(4.*COEP*EP/3.,0.25*EP))
ENDIF
```

**Validation**

The model implementation has been validated successfully for channel and pipe flow, flow past a backward facing step in a channel, the turbulent plane and round jet, 2d flow over a surface-mounted square rib, and 3d flow past a surface-mounted cube. Time constraints have precluded the performance of systematic grid-sensitivity studies for these cases. Typically, the realisable model increases the computational requirements by 35% compared to the standard k-ε model.

The model converges readily with inertial relaxation on k and ε of the same magnitude as the momentum equations. The exception was the plane and round jet, which exhibited convergence difficulties due to the large velocity gradients associated with the assumption of a uniform discharge velocity. These problems were cured easily by using linear relaxation of 20% on the turbulent kinematic viscosity ν<sub>t</sub> and setting an upper limit on ν<sub>t</sub> to prevent non-physical values arising during the course of convergence.

**Backward Facing Step:** The first case is 2D flow over a backward facing step in a channel with an expansion ratio of 1.5. The Reynolds number is 45,000 based on step height H. Step and outlet planes are located 4H and 20H downstream of the inlet, respectively.

A mesh of 50 vertical by 60 axial cells was used in the simulations. Figure 1 shows the velocity vectors predicted by the realisable k-ε model, and it can be seen that the edge of the step provides a fixed point of flow separation with a substantial recirculation zone downstream of the step.

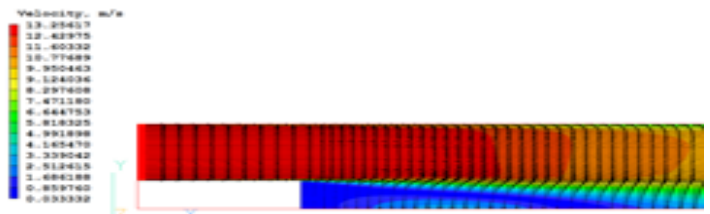


**Fig 1: Backward Facing Step: Velocity vectors and separation zone.**

Table 1 compares measured and calculated reattachment lengths behind the step. It is clear that the standard k-ε model underestimates the reattachment length by about 18%. RNG and Chen Kim models procure agreement to within 7% of the data, but superior predictions are obtained with the realisable model, which produces excellent agreement with the data.

	Realisable k-ε	Standard k-ε	Chen-Kim k-ε	RNG k-ε	Data
X <sub>R</sub> /H	7.0	5.8	6.6	6.6	7.1

**Table 1: Backward Facing Step: Measured and predicted reattachment lengths.**

**Channel and Pipe Flow:** For fully-developed turbulent channel and pipe flow at a Reynolds number of 10<sup>5</sup>, Table 2 compares predicted and measured values of the Darcy friction factor and the velocity-defect parameter. In the Table, U<sub>m</sub> is the centre-line velocity, U<sub>b</sub> is the bulk velocity, U\* (=√τ/ρ) is the friction velocity, where τ is the wall shear stress, and the friction factor f is defined by f=8(U\*/U<sub>b</sub>)<sup>2</sup>.

	Channel Flow	Pipe Flow	Channel Flow	Pipe Flow
	(U <sub>m</sub> -U <sub>b</sub> )/U*		Friction factor f	
Standard k-ε model	2.25	3.50	0.016	0.018
Realisable k-ε model	2.52	3.88	0.015	0.017
Experiment	2.32	3.75	0.016	0.018

**Table 2: Channel and Pipe flow: Measured and predicted friction factor and velocity-defect parameter**

It is clear that both sets of model predictions are in good agreement with the measured flow parameters. The larger values of the velocity-defect parameter produced by the realisable k-ε model are associated with the fact that the model predicts a somewhat larger value of  $C_{\mu}$  from equation (6) in core of the flow.

**Plane and Round Jet:** Table 3 compares the measured and predicted spreading rates of plane and round jets issuing into stagnant surroundings.

	Plane Jet	Round Jet
Standard k-ε model	0.101	0.112
Realisable k-ε model	0.103	0.098
Experiment	0.105-0.11	0.086 - 0.095

**Table 3: Plane and Round Jets: Measured and predicted spreading rates**

The table shows that standard and realisable models both predict the correct spreading rate of the plane jet, but the standard model seriously overestimates the spreading rate of the round jet. This large discrepancy with measurements is almost removed by the realisable k-ε model.

**Flow over a surface-mounted square rib:** The case considered is 2d, steady, turbulent flow past a surface-mounted square rib in a channel. The height H of the rib is 8.5% of that of the channel, and the Reynolds number based on channel bulk velocity and rib height is 300,000. The inlet plane is located 6H upstream of the rib, and the outlet plane 20H downstream of the rib. A mesh of 36 vertical by 80 axial cells was used in the simulations.

For this case, the main parameter characterising separation is the length of the separation zone  $L_s$  behind the rib. Experimental and computed results for several turbulence models are shown in Table 4:

	Realisable k-ε	Standard k-ε	Chen-Kim k-ε	RNG k-ε	Kato-Launder k-ε	Data
$L_s/H$	13.7	6.0	16.1	13.0	11.2	11.3

**Table 4: Surface-mounted Square Rib: Measured and predicted separation lengths**

For this case the realisable model performs much better than the standard k-ε model, which seriously underestimates the separation length.

The realisable model performs similarly to the RNG model, but the best predictions are obtained with the Kato-Launder k-ε model of PHOENICS, which is designed to address the problem of excessive turbulent production in the stagnation region on the front of the rib.

**Flow past a surface-mounted cube:** The final case is 3D turbulent flow past a surface-mounted cube in a channel. The cube occupies 50% of the channel height. The Reynolds number based on channel bulk velocity and cube height H is 40,000. The inlet plane is located 7H upstream of the cube, and the outlet plane 10H downstream of the cube.

Only half the flow width is simulated due to symmetry, and a mesh of 40 lateral (X) by 40 vertical (Y) by 88 axial cells (Z) was employed in the computations. The width of the solution domain is 4.5H.

For simplicity, steady flow is presumed although it is known that flow separates in front of the cube to form a primary and secondary vortex, and the main vortex wraps as a horse-shoe around the cube into the wake. The flow separates at the front corners of the cube on the roof and side walls; then reattaches on the side walls but not on the roof.

A large separation region develops behind the cube which interacts with the horseshoe vortex. In experiments vortex shedding is observed from the side walls and, because of momentum exchange with the wake, this leads to a shorter separation length than reported for a steady simulation.

For this case, the main parameters that characterise separation are the frontal stagnation point  $Y_s/H$ , the primary upstream separation point  $L_f/H$ , the roof reattachment point  $L_r/H$  and the length of the separation zone behind the cube  $L_b/H$ . Figure 2 shows the predicted velocity vectors at the channel mid-section, and the recirculation zones fore and aft of the cube are evident.

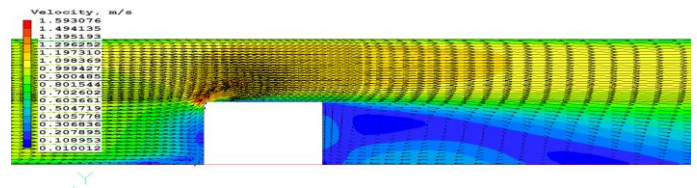


**Figure 2: Surface-mounted Cube: Velocity vectors and separation zones fore and aft of the cube at the channel mid section.**

Table 5 compares experimental and computed results of  $L_b/H$  for several turbulence models.

	Realisable k-ε	Standard k-ε	Chen-Kim k-ε	RNG k-ε	Kato-Launder k-ε	Data
$L_b/H$	2.2	1.85	2.35	2.27	2.62	1.65

**Table 5: Surface-mounted cube: Measured and predicted separation lengths behind the cube.**

Results shown in Table 5 are not grid independent, and the mesh is not fine enough to resolve the expected separation on the roof, or to capture adequately the primary upstream separation region. All models overpredict  $L_b$ , and the standard model gives closest agreement with the data. The modified models produce longer separation regions than the standard model because of their tendency to predict lower eddy viscosities in separated flow regions.

Although the present computations employ insufficient mesh resolution, it seems likely that inclusion of unsteady effects is required to effect a significant improvement in prediction of separation length. The use of very fine meshes in the important near-wall regions requires careful consideration because of the strong possibility of invalidating the high-Reynolds-number wall functions used in the present simulations.

**Conclusions**

The realisable  $k-\epsilon$  model has been implemented into the PHOENICS code by use of INFORM and PIL commands in the Q1 input file. The model implementation has been validated for a number of cases with good convergence and reasonable results. The realisable model performs better than the standard  $k-\epsilon$  model and its variants for the backward-facing step, the turbulent round jet, and flow past a square rib. For other cases, the model performs similarly to the more economical Chen-Kim and RNG variants of the  $k-\epsilon$  model. Now that the basic model testing is complete, there is scope to improve the present implementation by eliminating whole-field storage of some of the auxiliary variables. The model could also be exercised for 3D industrial and wind-engineering applications.

**References**

1. Shih, T.-H., Liou, W.W., Shabbir, A., Yang, Z. & Zhu, J. "A New  $k-\epsilon$  Eddy-Viscosity Model for High Reynolds Number Turbulent Flows - Model Development and Validation. Computers Fluids, 24(3):227-238, (1995).

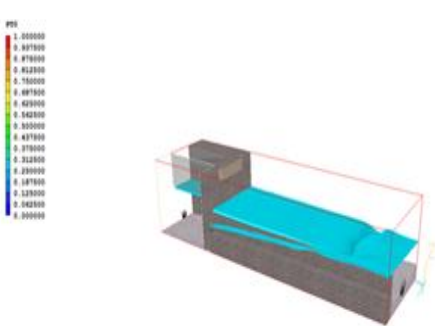
*Please share your experiences of PHOENICS by sending articles for inclusion in the Summer Newsletter, in Word format, to [newsletter@cham.co.uk](mailto:newsletter@cham.co.uk) Thank you.*

**WRc Innovation Day 2015**



Andrew Carmichael and James Stewart recently exhibited CHAM's CFD / PHOENICS technology at the WRc (Water Research Council) Innovation Day. The theme was **Innovation in Action** within the Water, Waste Management and Gas industries.

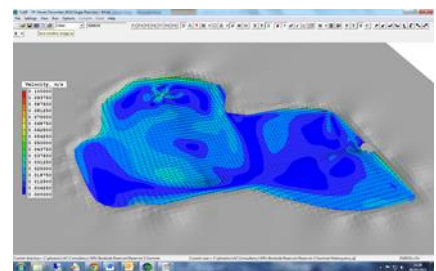
CHAM and WRc have a long-standing relationship and have worked together on numerous projects. Most recently CHAM was responsible for providing CFD expertise to model the flow within a new and innovative Combined Sewer Overflow (CSO) Chamber designed by WRc. In addition to CHAM presenting images and animations of the CFD modelling results, WRc had a physical model of the new CSO chamber design present on the day.



*CSO Computational Image*



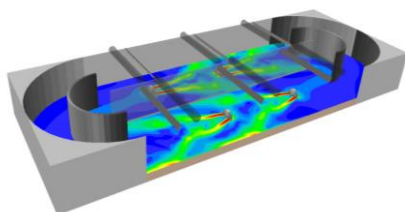
*CSO Physical Model*



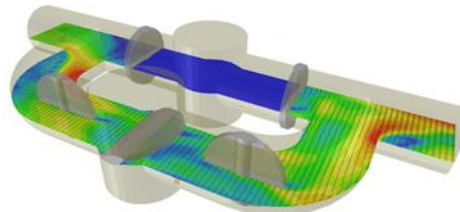
*Bankside Reservoir*

Over 70 suppliers and manufacturers demonstrated how their designs and technologies provide innovative solutions to problems in industry and some 300 guests attending on the day. In addition to the exhibitions and demonstrations there were speakers from each industrial sector who gave insightful presentations into the issues and challenges faced within industry.

As a collaborative partner of WRc, CHAM was given a stand in the *Showcase Marquee* to exhibit **PHOENICS** and showcase the work CHAM has undertaken in partnership with WRc and to demonstrate CFD applications across the Water industry



*Impeller Model of Wastewater surface*



*Fluid flow through a Pipe Geometry*